Article

Not peer-reviewed version

Development of an Automotive-Relevant Recycling Process for Paper Fiber-Reinforced Polypropylene Composites

Cecile A Grubb , Mahshid Mokhtarnejad , John Greene , John Misasi , David J Keffer , Marton Kardos , Hendrik Mainka , David P Harper *

Posted Date: 24 October 2024

doi: 10.20944/preprints202410.1946.v1

Keywords: recycling; polypropylene, natural fiber composites; paper fibers; injection molding; sustainability; automotive

Article

Development of an Automotive-Relevant Recycling Process for Paper Fiber-Reinforced Polypropylene Composites

Cecile A. Grubb [1,2,3], Mahshid Mokhtarnejad [2], John Greene [1], John Misasi [4], David J. Keffer [3], Marton Kardos [2], Hendrik Mainka [2] and David P. Harper [1,*]

[1] Center for Renewable Carbon, University of Tennessee Institute of Agriculture, Knoxville, TN 37996
[2] Volkswagen Group of America, Knoxville, TN 37920
[3] Department of Materials Science and Engineering, University of Tennessee, Knoxville, TN 37996
[4] Department of Engineering and Design, Western Washington University, Bellingham, WA 98225
* Correspondence: dharper4@tennessee.edu

Abstract: The automotive industry is under growing pressure from regulatory agencies to improve the recyclability of their plastic components. Simultaneously, manufacturers are adopting natural fiber composites in vehicles to reduce carbon footprints and decrease reliance on petroleum-based materials. This presents a challenge at vehicle end-of-life however, as natural fiber-reinforced polymers are substantially more difficult to recycle than their unreinforced counterparts. This study investigated the development of a mechanical recycling process for paper fiber-reinforced polypropylene composites, focusing on the impact of injection molding parameters—specifically, injection temperature and rate—on the thermal, mechanical, and water uptake properties of the composites. The results showed that processing temperature had a greater influence on composite performance than injection rate, with some limited interaction effects between the two. Higher processing intensity damaged the paper fibers, increasing the number of nucleation sites and resulting in greater polypropylene crystallinity. These structural changes reduced tensile properties at higher intensities, while flexural properties improved. Objective function analysis was applied to identify optimal processing conditions, balancing these competing trends. Overall, the findings demonstrate that paper fiber-reinforced polypropylene composites can be recycled into automotive relevant injection molding compounds using conventional plastic manufacturing techniques, though careful tuning of processing parameters is essential to achieve optimal performance.

Keywords: recycling; polypropylene; natural fiber composites; paper fibers; injection molding; sustainability; automotive

1. Introduction

The automotive industry has become increasingly interested in using natural fiber reinforced composites in recent years, as the industry moves toward a goal of net-zero carbon emissions by the mid-twenty first century. Natural fibers offer advantages over conventional reinforcement materials, such as glass or carbon, including comparatively low cost, low density, favorable acoustic properties, wide global availability and inherently low carbon footprint [1,2]. There are considerable disadvantages associated with natural fibers however, such as material variability, high moisture sensitivity, low microbial resistance, low degradation temperature, and limited compatibility with polymer matrices [3–6]. The low thermal stability of natural fibers in particular presents a problem for recycling, as reprocessing via standard polymer manufacturing techniques can lead to significant fiber degradation and poor material performance [7]. New European Union (EU) regulations require automotive manufacturers to increase the circularity of vehicle materials, with a specific focus on

 doi:10.20944/preprints202410.1946.v1

ensuring that plastic used in vehicles comes from recycled sources and is recyclable at a vehicle's end-of-life (EoL) [8].

Our previous work studied the viability of paper-based composites for automotive applications [9]. For the automotive industry, paper fibers offer benefits over other commonly used natural fibers such as hemp, flax, or jute. Paper is produced at a substantially larger volume than these other fibers, at 500 million tons per year in 2020, as opposed to flax (830,000 tons/year), jute (2.5 million tons/year), and hemp (215,000 tons/year) [10,11]. The pulp and paper industry also has well-developed quality control standards and methods which alleviate the variability issues typically seen with natural fibers [12]. Our previous study demonstrated that paper composites exhibit promising material properties, including flexural strength, impact resistance, and water uptake suitable for automotive applications. However, to ensure the successful commercialization of paper-based composites, a comprehensive evaluation of EoL pathways and recycling feasibility is imperative. This is particularly true for automotive parts intended for the European market, given the EU's forthcoming end-of-life vehicles (ELV) regulations [8].

As previously mentioned, natural fiber composites present unique recycling challenges due to their limited thermal stability. This is especially true when focusing on mechanical recycling methods like extrusion, injection molding or other techniques that involve melting and reforming the material, rather than chemically breaking down the polymer into monomers or other molecular components. Despite this, mechanical recycling remains the most studied type of recycling within the natural fiber composites community given its wide industrial applicability. A recent review from Zhao *et al.* describes the complex interplay of factors affecting recycled composite behavior, describing changes in properties such as mechanical behavior, thermal stability, crystallinity, hygroscopicity, durability during UV exposure, and rheological properties [13]. The general trends reported in the natural fiber recycling studies are presented in Table 1 below. It should be noted that different material systems can experience conflicting trends, as different polymers and fiber types can behave differently under identical conditions. For instance, Augier *et al.* report that a wood-filled PVC composite experiences an increase in glass transition temperature with mechanical recycling, likely due to polymer crosslinking, while other research shows that similar systems with different matrix materials, such as polypropylene (PP) or polylactide (PLA), instead display a decrease in glass transition temperature (T_g) due to chain scission during reprocessing [14].

Table 1. Reported material property changes during mechanical recycling of natural fiber composites.

Property		Reported Changes During Mechanical Recycling	Reference
Mechanical	Tensile	Both increase and decrease possible, decrease in properties attributed to polymer degradation and loss of fiber length while increase attributed to improved dispersion, increased crystallinity	[15–17]
	Flexural	Similar changes to tensile properties, although degradation and defects often had less of an impact	[18,19]
	Impact	Both increase or decrease in impact properties are possible; an increase attributed to the reduction in fiber length and increased ductility of the compound, a decrease attributed to increased crystallinity and associated brittleness	[18,20,21]
Thermal	Crystallization	Increase in crystallinity and shift to lower temperatures due to reduction in polymer chain length, increase in fiber surface area, increased nucleation, and oxidation of fibers	[17,18]
	Glass Transition	Both increase and decrease possible; decrease was attributed to reduced molecular weight from chain	[22,23]

 doi:10.20944/preprints202410.1946.v1

		scission, while increase was attributed to increase in molecular weight through crosslinking	
	Thermal Stability	Both increase and decrease possible, increases attributed to crosslinking of polymer, reduction in hemicellulose, and increase crystallinity; Reduction in thermal stability attributed to polymer matrix degradation and fiber degradation	[14,15,18]
Other	Hygroscopicity	Both increase and decrease possible; decrease results from improved dispersion within the polymer matrix and reduction in hemicellulose with an increase in cellulose surface oxidation while increases attributed to increased moisture penetration pathways from defects at polymer/fiber interface	[15,24]
	Rheological	Both increase and decrease are possible; a decrease in melt viscosity results from chain scission and a reduction in fiber length, increase is also possible due to an increase in surface area from fiber length reduction; Shear sensitivity may also increase	[15,17]

This research aims to develop a method for mechanically recycling paper fiber-reinforced polypropylene composites, mimicking industrial recycling processes to ensure compatibility with industry standards. Paper composite laminates were size-reduced and then compounded with additional polypropylene to produce an injection molding compound. This material was injection molded under various processing conditions to determine the bounds of the processing window. Thermal, mechanical, and moisture-uptake properties of the produced samples were studied to characterize trends in structure-property relationships of these composites. From this, processing conditions were identified that balance achieving a high degree of polymer crystallinity in the samples while minimizing fiber degradation, the combination of which results in optimal mechanical properties. We anticipate these results will pave the way for future adoption of both the virgin composite laminates and their recycled counterparts within the automotive industry.

2. Materials and Methods

2.1. Materials

The following materials were used as received: Domtar bleached hardwood kraft market pulp (MP) and MiniFibers precision cut 3 mm length, 15.3 μm diameter polypropylene (PP) fibers, isotactic PP pellets with a melt flow index (MFI) of 35, Honeywell AC950 propylene maleic anhydride copolymer (MAPP). Market pulp fiber dimensions were measured using a L&W Fiber Tester Plus, revealing a mean fiber length was 1.004 mm and a mean fiber width was 19.9 μm. Market pulp density was estimated to be 1.53 ± 0.05 g/cm^3 using a Micromeritics AccuPyc II 1340 gas pycnometer.

2.2. Recyclate Manufacturing

Recyclate was prepared for injection molding in such a way as to mimic an industrial process, aiming to achieve representative material properties. Composite laminates were produced from 60 wt.% paper fiber and 40 wt.% polypropylene fiber using the method described in our previous work [25]. Following compression molding, the laminates were shredded into flakes using Conair-Wortex granulator (model number: 933001). The flake was further size reduced using Thomas Model 4 Wiley Mill to obtain a low bulk density granulate.

MAPP was included in the formulation to improve compatibility between the paper fibers and polypropylene matrix. Therefore, the paper composite granulate was manually blended with PP pellets and MAPP pastilles to achieve a final mixture with a composition of 4.7 wt.% MAPP, 28.6 wt.% market pulp fiber, and 66.7 wt.% polypropylene (nominally 30% paper fiber/70% PP). This

 doi:10.20944/preprints202410.1946.v1

mixture was compounded in a 27 mm Leistriz twin screw extruder and pelletized using a BT 25 Lab Series Pelletizer for use in the injection molding stage of this study. An overview of the recycling process is shown in Figure 1.

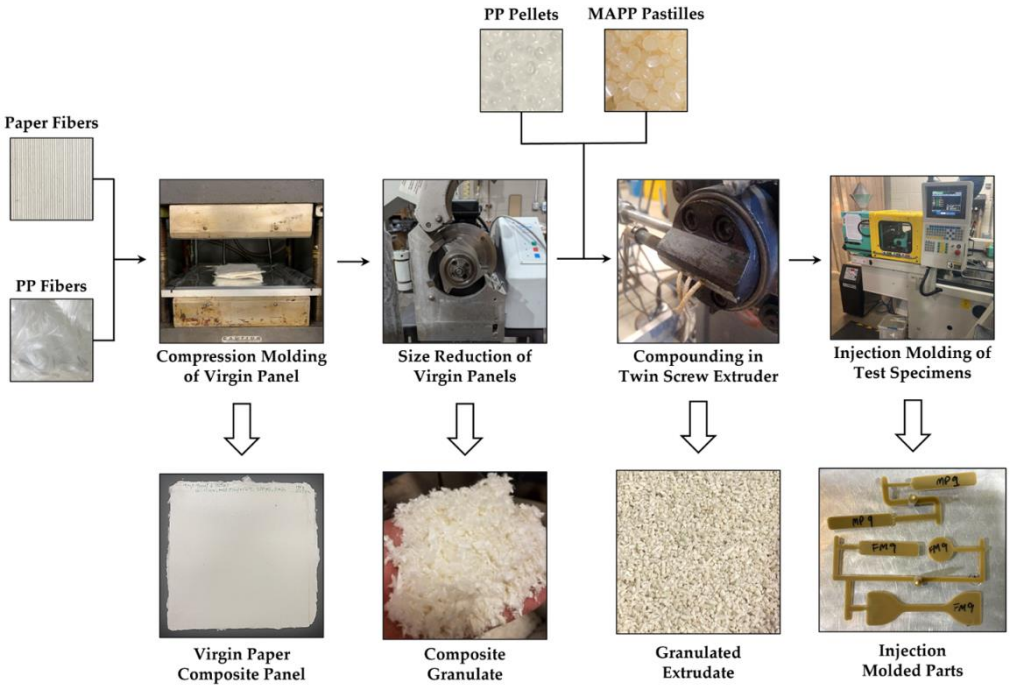

Figure 1. Overview of recyclate manufacturing and injection molding process and the products of each stage.

2.3. Injection Molding

Specimens were injection molded into a custom three-cavity mold designed to produce flexural, tensile and rheology test specimens. A 28-ton Arburg Allrounder machine equipped with a hot-air desiccant dryer and mold heating/cooling device was used for injection molding. To investigate the influence of processing parameters on the final product, injection rate and processing temperature were varied while all other processing variables were held constant at the values shown in Table 2. Other parameters maintained constant at injection pressure of 86.2 MPa (12,500 psi), shot size of 19.7 cm^3 (1.2 in^3), cooling time of 15 seconds, and cooling temperature of 35 °C (95 °F).

Table 2. Experimental conditions for different injection temperature and speed. Each set name represents a combination of injection temperature (°C) and injection speed (in^3/s).

Set Name	Injection Temperature (°C)	Injection Speed (in^3/s)
T200-I1	200	1
T200-I2	200	2
T200-I3	200	3
T200-I4	200	4
T210-I1	210	1
T210-I2	210	2
T210-I3	210	3
T210-I4	210	4
T220-I1	220	1
T220-I2	220	2
T220-I3	220	3
T220-I4	220	4

 doi:10.20944/preprints202410.1946.v1

T230-I1	230	1
T230-I2	230	2
T230-I3	230	3
T230-I4	230	4
T240-I2	240	2
T240-I3	240	3

2.4 Differential Scanning Calorimetry (DSC)

Differential scanning calorimetry was performed using a TA Q2000 to study the thermal behavior of the injection molded samples. Samples (5-10 mg) were cut from the injection molding runner system of the injection molded parts and subjected to a heating cycle from room temperature to 205 °C, followed by cooling to -25 °C, and a final heating cycle to 250 °C. All temperature scans were conducted at a rate of 5 °C/min under a nitrogen (N_2) atmosphere. The DSC data was analyzed to obtain melt temperatures (ΔT_m) and enthalpies (ΔH_m) reported for both heating cycles, and crystallization temperatures (ΔT_c) and enthalpies (ΔH_c) reported for the sole cooling cycle. A representative DSC curve is shown below in Figure 2 to demonstrate method by which temperatures and enthalpies were obtained.

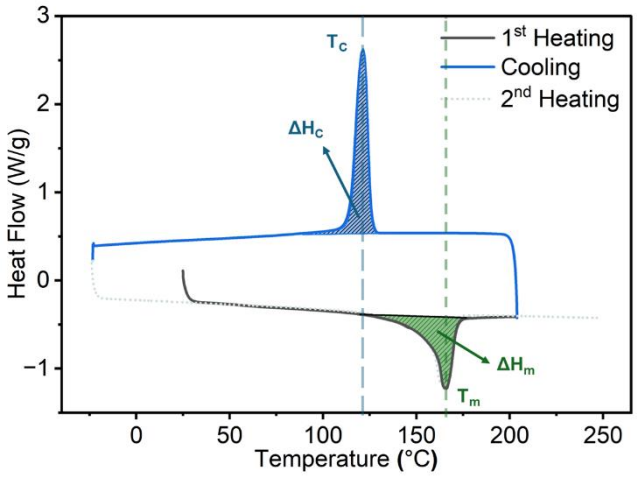

Figure 2. Example of DSC curve of paper-reinforced polypropylene composites to illustrate how enthalpies and temperatures were measured for each sample. The 2nd heating cycle is greyed out for clarity.

2.5. Thermogravimetric Analysis (TGA)

Thermogravimetric analysis was performed using a TA Q50 instrument to evaluate the thermal stability of the injection molded materials. Samples were ramped from room temperature to 600 °C at 10 °C/min under a N_2 atmosphere. The sample size was approximately 10 mg for all tests. As with the DSC testing, samples were obtained from the injection molding runner system. The TGA data was analyzed to obtain temperature at which 50% mass loss occurred (T_{50}) and residual mass.

2.6. Fourier Transform Infrared Spectroscopy (FTIR)

Attenuated Total Reflectance-Fourier Transform Infrared (ATR-FTIR) spectroscopy was performed using a PerkinElmer Spectrum Two FT-IR spectrometer to investigate the chemical composition and potential degradation of the injection molded parts. Testing was performed between 500 – 4000 cm^{-1} at a resolution of 4 cm^{-1} and 32 scans per spectrum. FTIR samples were prepared by slicing off thin pieces from the runner system using a precision utility knife.

2.7. Tensile Testing

 doi:10.20944/preprints202410.1946.v1

Tensile testing was performed in accordance with ASTM D638 using Type IV specimens. The samples measured 115 mm in overall length, 6.4 mm in width in the gauge region, and 2.2 mm in thickness. They were conditioned at 25 °C and 65% relative humidity for 88 hours prior to testing. Tensile testing was performed using an Instron 5567 universal testing machine equipped with self-centering wedge grips and 30 kN load cell. The crosshead speed during testing was set to 1.125 mm/min and strain was measured using clip on extensometer.

2.8. Flexural Testing

Flexural testing was performed in accordance with ASTM D790. Samples were conditioned using the same procedure described in the tensile testing section. Flexural testing measurements were taken using an Instron 5567 universal testing machine equipped with a 3-point bend test fixture and 500 N load cell. A test span of 45 mm and a test rate of 1.125 mm/min were used. Samples were tested until a 25% strain was reached. The Instron deflectometer used to measure strain was equipped with an extensometer with a 25 mm range. Flexural sample dimensions were approximately 60 × 12 × 3 mm.

2.9. Water Uptake Testing

Water uptake measurements were conducted using a modified ASTM D570 method, in which test specimens were 14 mm in length, 14 mm in width, and 2.4 mm in thickness, rather than standardized dimensions. Prior to testing, samples were dried overnight under vacuum at 80 °C to remove any excess moisture. Following the conditioning step, the samples were cooled in a desiccator unit and weighed using a precision analytical balance to establish an initial mass. For testing, samples were placed into a 23 °C water bath and mass was re-measured after 24 hours and 504 hours of submersion.

3. Results and Discussion

3.1. Recycling Process Development

The goal of this work was to develop industrially viable recycling processes for paper-reinforced polypropylene composites and identify limitations and challenges along the way. This started with the size reduction of the composite laminates. The initial effort focused on the use of a Conair-Wortex granulator, a commonly used equipment in the injection molding industry for regrinding production scrap to create post-industrial recyclate (PIR) [26]. However, the resulting "fluffy" flake posed challenges in material feeding during extrusion process due to their size. To address this, we therefore added a second step, in which we used a knife mill to further reduce the size of the granulate to ~ 4.5 × 2.5 × 1 mm. At this point, the granulate was still low-bulk density, but it fed into the extruder without bridging or clogging issues seen in previous tests.

Following size reduction, the granulate was compounded with polypropylene pellets and MAPP, the latter of which acted as a coupling agent between the paper fibers and polypropylene matrix. We processed the material under the lowest possible temperature profile in the twin screw extruder, detailed in Table 3. The reason for this was to minimize thermal degradation of paper fibers, while preventing excessive torque on extruder motor. The addition of MAPP was necessary to prevent severe "shark-skinning" of extrudate, a phenomenon that occurs due to melt fracture of the polymer when exiting the extruder die [27]. The extrudate was pelletized with an in-line unit, generating the feedstock for the subsequent injection molding stage.

 doi:10.20944/preprints202410.1946.v1

Table 3. Extruder processing parameters used for compounding of paper composite granulate with MAPP and PP.

Extruder Temperature Profile (°C)										Other Information	
Zone 1	Zone 2	Zone 3	Zone 4	Zone 5	Zone 6	Zone 7	Zone 8	Zone 9	Zone 10	Feed Rate (g/min)	Screw Speed (RPM)
50	80	90	100	100	200	210	210	210	200	20	150

As with extrusion, we aimed to injection mold the paper-polypropylene composite at the lowest possible temperature. This was ultimately determined to be 200 °C, as lower temperatures resulted in "short shots" – parts in which the material was unable to completely fill the mold cavity. From this baseline, we were able to investigate the different combinations of temperature and injection rate on the processability of the composite material, with the goal of identifying the upper limit of the processing window. The composite material processed well until we reached 240 °C, at which point we were only able to produce parts at injection rates of 32.8 – 49.2 ml/s (2 and 3 in^3/s), as the material would not inject properly at either 16.4 or 65.6 ml/s (1 or 4 in^3/s).

3.2. Impact of Injeciton Molding Parameters on Composite Thermal Behavior

The thermal properties of the injection molded specimens were measured using differential scanning calorimetry and thermogravimetric analysis. DSC was used to study the melting and crystallization behavior, while TGA was used to characterize the thermal stability of the materials. Figure 3 shows the results of the DSC testing, with melt temperatures and enthalpies reported for both heating cycles, and crystallization temperatures and enthalpies reported for the sole cooling cycle. TGA data is reported in supplementary information (Table S1), as no statistical significance was seen within the results.

Overall, thermal analysis shows subtle correlations between the processing conditions and the resulting properties. The most notable analysis outcome is the positive correlation between the processing temperature and both recrystallization temperature and enthalpy, seen in Figures 3C and 3D. Likewise, it appears that both of the recrystallization properties are positively correlated with injection rate, although this is more difficult to visually detect. The impacts of processing parameters on the melting temperature and enthalpy during both the first and second heating cycles are not visually obvious. Regression analysis was employed to further elucidate the complex relationships between processing parameters and material properties. For this, we considered both linear (temperature, injection rate) and interactions between the two (temperature*injection rate) terms. The p-values for each term are presented in Table 4, where bold values indicate statistical significance at a level of $p < 0.05$. Additionally, Table 4 includes the direction of correlation (↑ for positive, ↓ for negative) for all statistically significant terms.

The processing temperature has the most significant impact on melting and recrystallization behavior of the samples. Within the melting behavior, the processing temperature is positively correlated with the melting enthalpy on the first heat cycle and negatively correlated with the re-melting temperature on the second heat cycle. It is also positively correlated with both the recrystallization temperature and recrystallization enthalpy. ΔH_m (1st heat) corresponds with the thermal history from cooling the polymer in the injection molding tool. At higher processing temperatures, the polymer reaches a lower viscosity during injection molding. This improves the ability of the polymer to crystallize while cooling due to improved chain mobility with decreased viscosity [28].

The inverse correlation between processing temperature and with T_m (2nd heat) is likely due to a decrease in PP molecular weight from thermo-oxidative degradation. Previous literature has noted that that polypropylene molecular weight is relatively stable up to processing temperatures of 230 °C, however above this point chain scission rises rapidly increasing temperature [29]. These changes in molecular weight are not apparent in the first heating cycle as the effects are masked by the different temperature differentials ($\Delta T = T_{process} - T_{room\ temperature}$) associated with different processing temperatures during injection molding, which leads to disparate cooling experiences

 doi:10.20944/preprints202410.1946.v1

between different processing conditions. Conversely, the cooling cycle in the DSC leads to uniform thermal histories and reveals the differences between melting temperatures during the second heating cycle. The positive correlation between processing temperature and recrystallization behavior (Tc and ΔH_C) is also likely due to this decreasing molecular weight, which allows for improved nucleation of PP crystals during cooling.

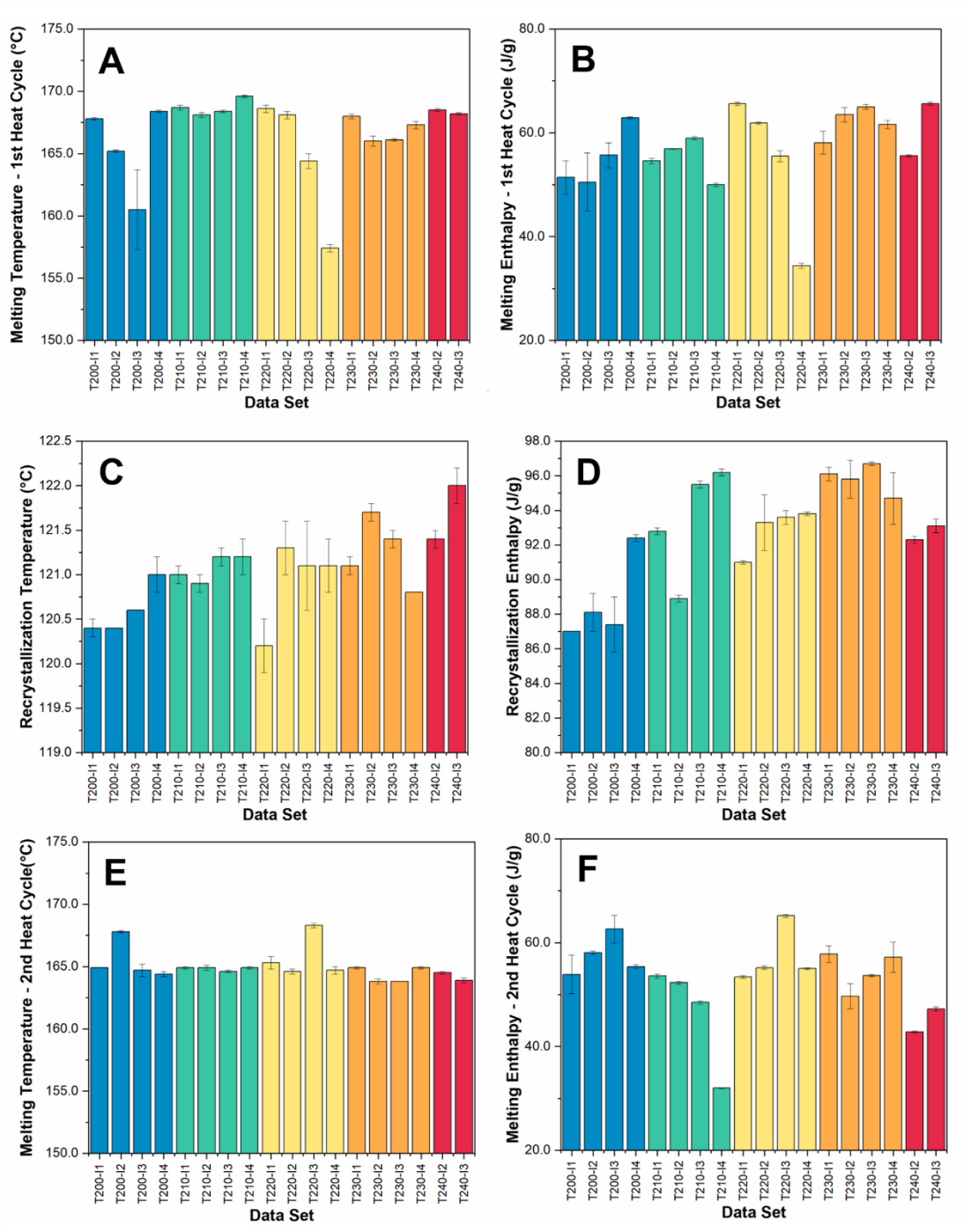

Figure 3. Thermal properties of injection molded samples: (A) Melting temperatures of the 1st heat cycle, (B) melting enthalpies for the 1st heating cycle, (C) recrystallization temperatures, (D) recrystallization enthalpies, (E) melting temperatures of the 2nd heat cycle, and (F) melting enthalpies for the 2nd heating cycle.

 doi:10.20944/preprints202410.1946.v1

Table 4. P-values and correlation direction for the effects of temperature, injection rate, and their interaction on thermal properties.

		P-Values			Correlation Direction		
Test Method	Property	Temp.	Injection Rate	Temp.* Injection Rate	Temp.	Injection Rate	Temp.* Injection Rate
DSC	T_m (1st Heat)	0.59607	**0.00972**	0.25472	-	↓	-
	ΔH_m (1st Heat)	**0.02989**	0.08279	0.08824	↑	-	-
	T_m (2nd Heat)	0.04818	0.67182	0.33610	↓	-	-
	ΔH_m (2nd Heat)	0.24570	0.29333	0.48744	-	-	-
	T_c	**<0.0001**	**0.01404**	0.25712	↑	↑	-
	ΔH_c	**<0.0001**	**0.00612**	**0.02801**	↑	↑	↑
TGA	T_{50}	0.34323	0.13614	0.54321	-	-	-
	Residual Mass	0.21116	0.21116	0.38690	-	-	-

The injection rate shows less statistically significant impact on the thermal properties, however there are a few key relationships that can be observed. The injection rate is negatively correlated with T_m on the first heating cycle only, while it is positively correlated with both T_c and ΔH_c. The injection rate and associated shear likely have a greater impact on the reinforcing fibers than the polymer matrix and would be expected to decrease the fiber length, in turn increasing the number of nucleation sites available. The increasing shear rate also favors the formation of β-phase crystalline structure in the polypropylene matrix [30]. The combination of these two effects explains both the changes in melting temperature and recrystallization behavior. The increase in nucleation sites will improve nucleation efficiency, increasing the crystallization rate and resulting in the corresponding increase in crystallization temperature and enthalpy [22]. Likewise, the β-crystals of polypropylene are known to melt at a lower temperature than α-crystals, hence the depression of melt temperature [31]. This effect is only seen in the first heat cycle, however, as there are no shear forces during the DSC experiment to re-induce the β crystallite structure.

3.3. Impact of Injeciton Molding Parameters on Chemical Composition of Composites

FTIR was used to analyze the chemical changes in the injection molded samples. This technique measures the characteristic vibrational frequencies of molecules, allowing for identification of various functional groups present in the composites. The peaks of interest were identified as 3330 cm^{-1} (O-H stretch), 2917 cm^{-1} (C-CH_3 stretch), 1761 cm^{-1} (C=O stretch), 1656 cm^{-1} (enolic groups), 1456 cm^{-1} (CH_2 bend), 1375 cm^{-1} (CH_3 bend), 1033 cm-1 (C-O stretch) [32]. An example plot with these peaks highlighted is shown in Figure 4. We chose to normalize against the C-CH_3 peak at 2917 cm^{-1} for further analysis, as it appears in all the raw materials and is not expected to change significantly with oxidation. The carbonyl index (CI), a measure of the relative amount of carbonyl groups (C=O) present in the material, was calculated for each sample using Equation 1.

$$CI = \frac{Intensity\ of\ 1761\ cm^{-1}}{Intensity\ of\ 1456\ cm^{-1}} \quad (1)$$

The full results of both the normalization and CI calculation are included in the supplemental analysis; however, Figure 5 shows the trends observed in the samples molded at 2 in^3/s which are representative of the overall trends observed across all injection rates. Finally, as with the thermal

 doi:10.20944/preprints202410.1946.v1

analysis, regression analysis was used to determine the statistical impact of the processing parameters on studied peak intensities and CI values. The p-values and correlation directions for this analysis are reported in Table 5.

Table 5. P-values and correlation directions for the effects of temperature, injection rate, and their interaction on FTIR peak intensities.

	P-Values			Correlation Directions		
Peak Number	Temp.	Injection Rate	Temp.* Injection Rate	Temp.	Injection Rate	Temp.* Injection Rate
1033	0.2827	0.6382	0.2174	-	-	-
1375	**0.0277**	0.1243	0.3028	↑	-	-
1456	**0.0209**	0.5179	0.7500	↑	-	-
1656	**0.0051**	0.7285	0.7555	↑	-	-
1761	**0.0057**	0.6360	0.7259	↑	-	-
3330	0.4062	0.5064	0.2623	-	-	-
Carbonyl Index	**0.0481**	0.9432	0.9975	↑	-	-

Overall, the injection molding temperature was the only processing parameter that had a statistically significant impact on the chemical composition of the samples. Increasing injection molding temperature led to increases in all FTIR peaks associated with degradation, as well as a pronounced rise in the carbonyl index. The peak at 1761 cm^{-1} is associated with the formation of carbonyl groups during oxidative degradation of both polypropylene and paper fibers [33,34]. The 1656 cm^{-1} peak is associated with the formation of enolic or conjugated ketone groups during cellulose oxidative and hydrothermal degradation [35]. The peaks at 1465 and 1375 cm^{-1} are associated with CH_2 scissoring and C-H bending in cellulose and are strongly correlated with cellulose crystallinity [36]. When the paper fibers are exposed to a thermo-oxidative environment, the amorphous regions of the cellulose will degrade at lower temperatures, leaving behind a larger portion of the crystalline cellulose, thus resulting in increases in the 1465 and 1375 cm^{-1} peaks. Similar effects have been seen in wood degradation, although they were outsized in comparison to this study, as wood has a much higher lignin and hemi-cellulose content than the paper fibers used in this study [37]. Overall, the FTIR results suggest that the material experiences a higher degree of oxidative degradation with increased temperature, as would be expected. Furthermore, the results seem to suggest that the oxidative degradation primarily affects the paper fibers rather than the polypropylene matrix.

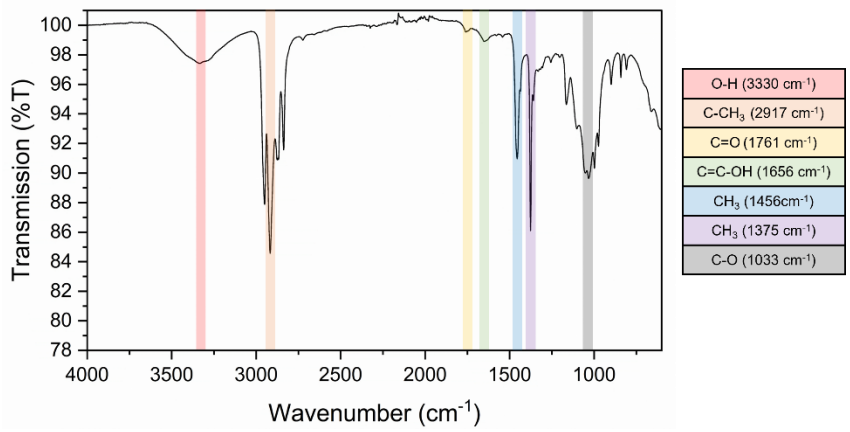

Figure 4. Example spectra of T230-I2 with relevant peaks identified.

Preprints.org (www.preprints.org) | NOT PEER-REVIEWED | Posted: 24 October 2024 doi:10.20944/preprints202410.1946.v1

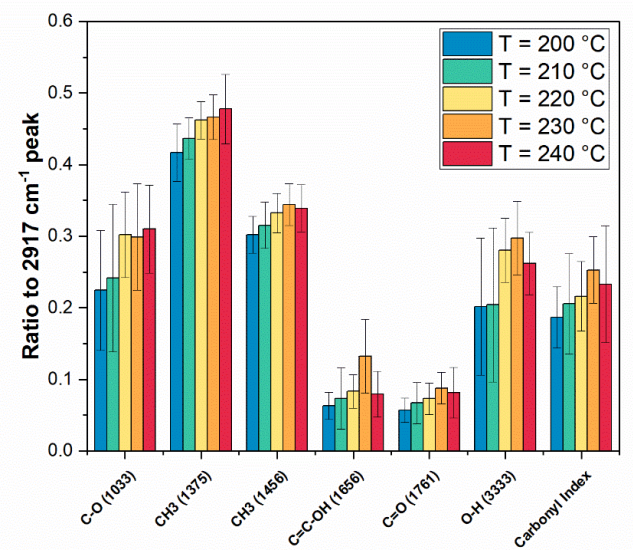

Figure 5. Ratio of intensities of various peaks to intensity of C-CH_3 peak at 2917 cm^{-1}. Trends are shown only for samples molded at an injection rate of 2 in^3/s, as they are representative of other injection rates. .

3.4. Impact of Injection Molding Parameters on Composite Mechanical Behavior

The mechanical behavior of the composites was studied using flexural and tensile analysis. For both methods, the modulus, strength, and strain at failure were recorded as these properties are critical for composite part performance in automotive applications. In particular, the moduli and strength are used as design criteria. The three measured properties are shown in Figures 6 for both tensile and flexural testing. The same method of regression analysis as previously described was used to determine statistical significance of processing parameters. The p-values for this analysis are reported in Table 6. Analysis of variance (ANOVA) was used to determine statistically different pairs via the Tukey-Kramer test, the results of which are included in Figure 6.

Table 6. P-values and correlation direction for the effects of temperature, injection rate, and their interaction on mechanical properties.

		P-Values			**Correlation Directions**		
Test Method	Property	Temp.	Injection Rate	Temp.* Injection Rate	Temp.	Injection Rate	Temp.* Injection Rate
Tensile	Young's Modulus	**0.02119**	**0.02684**	0.30428	↑	↓	-
	Ultimate Tensile Strength	**<0.0001**	**0.00988**	0.33631	↓	↓	-
	Tensile Strain at Break	**<0.0001**	0.0901	0.1152	↓	-	-
Flexural	Flexural Modulus	0.4386	0.1216	**0.0245**	**-**	**-**	↑
	Flexural Strength	0.7940	0.1203	**0.0042**	**-**	**-**	↑
	Flexural Strain at Max Stress	**<0.0001**	0.0533	**0.0156**	↓	-	↑

Both processing temperature and injection rate were statistically significant for the tensile strength and modulus the composites, while only temperature had a statistically significant effect on strain at break. Tensile modulus was positively correlated with temperature and negatively correlated with injection rate, while the tensile strength was negatively correlated with both parameters. It should be noted that the interaction term (temperature*injection rate) was not statistically significant, which indicates that these two variables do not interact with each other in a

 doi:10.20944/preprints202410.1946.v1

meaningful way. Tensile strain at break was also negatively correlated with temperature, similar to ultimate tensile strength.

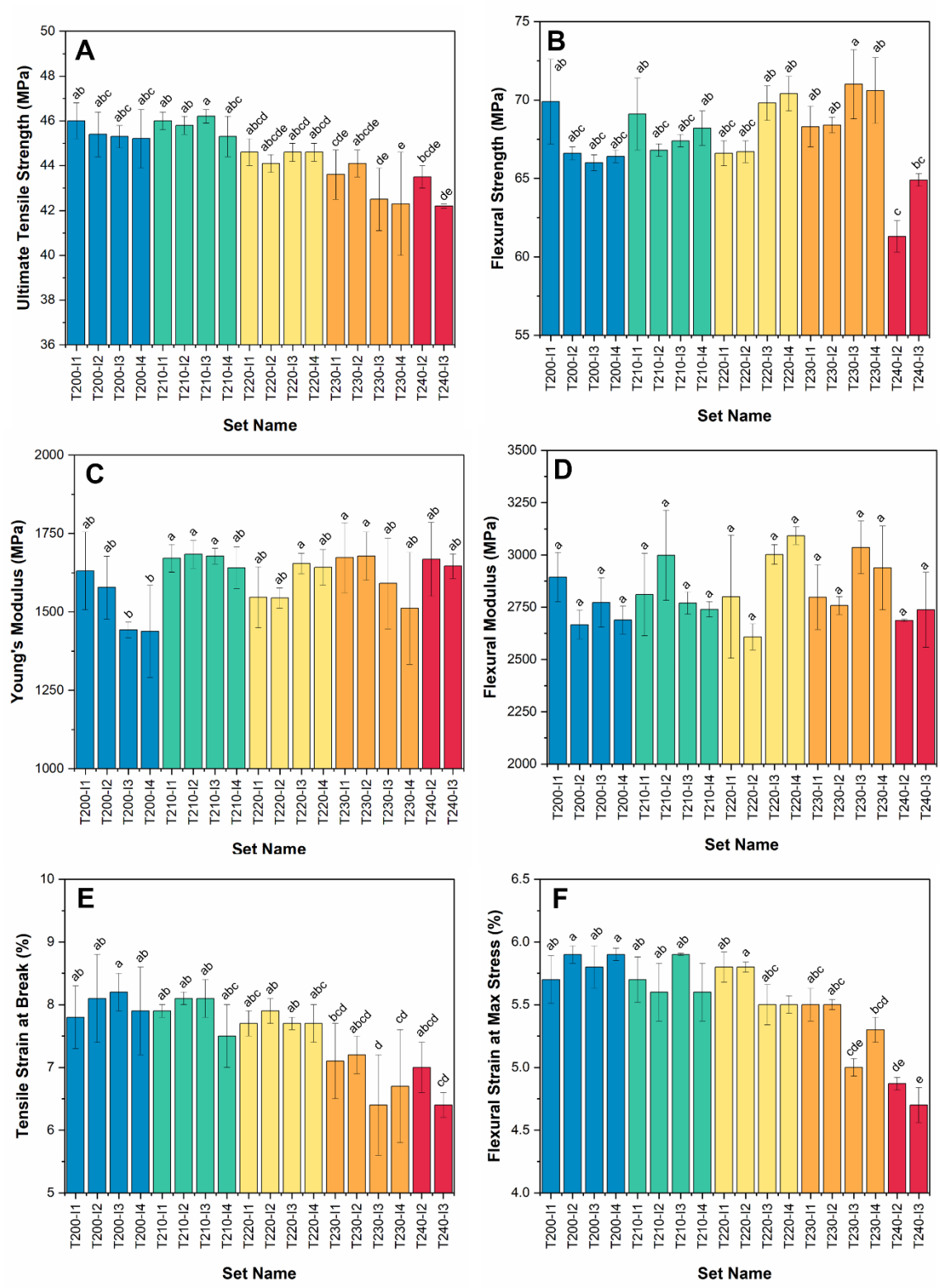

Figure 6. Mechanical properties of injection molded specimens: (A) ultimate tensile strength, (B) flexural strength (B) Young's modulus, (D) flexural modulus, (E) tensile strain at break and (F) flexural strain at maximum stress. Different letters (i.e., a,b,c,d, and e) designate statistically different data sets at $p < 0.05$.

 doi:10.20944/preprints202410.1946.v1

The increase in tensile modulus with increasing temperature can likely be attributed to the increase in crystallinity, as PP crystallinity is well-known to correlate with Young's modulus [38]. This is further corroborated by the thermal analysis data, indicating that increasing processing temperature led to higher crystallinity. Higher crystallinity within the matrix can also explain the observed decreases in tensile strength and strain at break. This is a direct consequence of increased modulus for strain at break – as the composite becomes stiffer, it will also become more brittle [39]. The decrease in tensile strength with increasing temperature can also be associated with this increased crystallinity, as smaller and weaker amorphous fractions must account for most of the composite strain [40]. This ultimately leads to brittle failure at lower stress. The reduction in modulus and strength associated with increasing injection rate can also be attributed to fiber length reduced by increased shear forces during injection molding [21,41].

The trends observed in flexural properties were somewhat different than those seen in the tensile properties of the composite material. Only flexural strain at maximum stress was correlated with a primary factor – a negative correlation with processing temperature. Neither temperature nor injection rate was directly correlated to either flexural strength or modulus, however the interaction term was positively correlated with all three measured properties. In general, flexural strength appears to stay relatively constant with increasing temperature, however this trend abates once we reach a processing temperature of 240 °C, at which point the flexural strength drops significantly. This indicates that flexural strength is less sensitive to the degradation that is occurring until a threshold is reached, unlike tensile strength which drops off in a more linear fashion. These contrasting observations can be explained through the inherent differences between tensile and flexural testing. Tensile tests apply uniform stress throughout the cross-section of the materials, whereas flexural tests concentrate stress on the surfaces of the specimen. This also explains why flexural strengths are typically higher than tensile strengths for a given material [42]. The positive correlation between the interaction term (temp.*injection rate) is likely due to decreased viscosity of the polymer under more intense processing conditions. The improved flow of the polymer will lead to better surface properties thereby improving flexural strength, although at very intensive processing conditions the degradation to the fibers is more significant than these positive effects. This is likewise true for the flexural modulus; however, we do not observe a drop off in the stiffness of the material as this is less sensitive to defects in the bulk material than the strength. Flexural strain at maximum stress experiences similar trends to tensile strain at break and can again be attributed to increasing matrix crystallinity.

The analysis of variance between the different data sets revealed that although the processing conditions are having statistically significant effects on the trends within the material properties, the actual values of the mechanical properties do not change significantly throughout the processing window studied. This is particularly true for the stiffness of the material with all the flexural moduli falling within a statistically equal range and the tensile Young's modulus only has a few data sets that are not statistically equivalent. From a manufacturing perspective, this suggests the recyclate is tolerant of a wide processing window, although there is an upper limit to the temperature that it can endure.

3.5. Impact of Injeciton Molding Parameters on Composite Water Uptake Behavior

The water absorption behavior of the injection molded samples was measured to assess their resistance to humid environments, a common challenge for natural fiber composites. The samples exhibited a low water uptake, with an average mass increase of 0.4 ± 0.2 wt.% after 24 hours of submersion and 0.7 ± 0.4 wt.% after 504 hours of submersion. The processing conditions had no statistically significant effect on water uptake behavior, as all the p-values were far greater than 0.05, as shown in Table 7. A significant degree of variability was observed, likely due to limitations of the resolution of the scale used for these measurements. Overall, these tests indicate that paper fibers were almost entirely encapsulated by the polypropylene matrix, thereby preventing moisture ingress into the fibers.

 doi:10.20944/preprints202410.1946.v1

Table 7. P-values and correlation direction for the effects of temperature, injection rate, and their interaction on water uptake behavior.

Test Method	Property	Temp.	Injection Rate	Temp.*Injection Rate
Water Uptake	24 Hour Water Uptake	0.3451	0.3428	0.3804
	504 Hour Water Uptake	0.2491	0.6949	0.1681

3.6. Correlation between Crystallinity and Mechanical Properties

Multivariate analysis was used to analyze the relationship between crystallinity and mechanical properties to understand underlying correlations. The Pearson's correlation coefficient from this analysis are shown in Table 8, with associated p-values reported in the supplementary info. T_m (2^{nd} heat) and ΔH_m (2^{nd} heat) were not included in this analysis, as they do not correspond to the thermal history associated with processing the tested specimens. These relationships were analyzed and no correlations were observed. In general, Pearson's correlation coefficients with an absoluate value between 0.00 – 0.09 are considered to have a negligible correlation, those from 0.10 – 0.39 are weakly correlated, 0.40 – 0.69 moderately correlated, 0.70 – 0.89 strongly correlated, and 0.90 – 1.00 very strongly correlated [43].

The majority of the correlation coefficients generated by the multivariate analysis fall in the negligible to weakly correlated range, however there are a number of notable exceptions. Ultimate tensile strength is very strongly correlated with tensile strain at break, strongly correlated with flexural strain at maxium stress, and moderately negatively correlated with ΔH_m (1st heat), T_c and ΔH_c. Tensile strain at break is also strongly correlated with flexural strain at maxiumum stress, and moderately negatively correlated with T_c and ΔH_c. Flexural modulus shows a moderate negative correlation with T_m (1st heat), while flexural strain at max stress is shows a moderate positive correlation.

Table 8. Pearson's correlation coefficients from multivariate analysis, with moderate or better correlation bolded for clarity. .

	Young's Modulus	UTS	Tensile Strain	Flex. Modulus	Flex. Strength	Flexural Strain	T_m (1st heat)	ΔH_m (1st heat)	T_c	ΔH_c
Young's Modulus	1	0.0714	-0.1452	0.2315	0.0538	-0.3114	0.186	-0.2378	0.3715	0.2928
UTS	-	1	**0.9133**	-0.099	0.0158	**0.8053**	-0.0166	**-0.4111**	**-0.5236**	**-0.4359**
Tensile Strain		-	1	-0.1793	-0.0814	**0.8770**	-0.1767	-0.3841	**-0.5601**	**-0.5159**
Flex. Modulus	-	-		1	**0.6753**	-0.2114	**-0.4532**	-0.3306	-0.1093	0.1061
Flex. Strength	-	-		-	1	0.1736	-0.2695	-0.2194	-0.1716	0.3155
Flexural Strain						1	**0.5959**	-0.1966	**-0.6315**	-0.2987
T_m (1st heat)	-	-		-	-		1	**0.5959**	0.1079	0.1637
ΔH_m (1st heat)	-	-		-	-		-	1	0.2694	0.178
T_c	-	-		-	-		-	-	1	**0.6084**

 doi:10.20944/preprints202410.1946.v1

ΔH_c	-	-		-	-		-	-	-	1

*UTS = Ultimate Tensile Strength. T_m = melt temperature, T_c = crystallization temperature, ΔH_m= melt enthalpy, ΔH_c = crystallization enthalpy

These correlations give further insight into the relationship between polymer morphology and mechanical behavior. In particular, these results suppor the conclusion that degree of crystallinity and type of crystal are having significant impacts on material strength and brittleness. Degree of crystallinity is directly measured by both ΔT_c and ΔH_c. The inverse correlation between these two properties and ultimate tensile strength further confirms the previously hypothesized relationship. Likewise, the inverse correlation between tensile strain at break and both ΔT_c and ΔH_c further suggests that increasing polymer crystallinity is causing the composites to become more brittle. The relationships between melting temperature and both flexural modulus and flexural strain at maximum stress suggest that the increase in β crystalline regions within the polypropylene matrix is impacting the stiffness and brittleness of the composite. The β crystal morphology appears to have a negative impact on stiffness, while increasing the ductility of the material.

3.7. Identification of Optimal Injection Molding Processing Conditions

A set of optimal processing conditions was selected by comparing the mechanical properties (ultimate tensile strength, Young's modulus, flexural strength, flexural modulus) associated with different processing conditions, as well as their standard deviations. This comparison was done using objective function minimization, which aligns with our previous work. The objective function was defined as

$$f_{obj}(s_j) = \sum_{i=1}^{n_{prop}} w_i \left(\frac{p_{i,j}}{\langle p_i \rangle}\right)^{n_i} \quad (1)$$

where n_{prop} is the number of properties ($n_{prop} = 8$), $p_{i,j}$ is the value of property i for sample j, $\langle p_i \rangle$ is the average value of property i over all samples, w_i is the relative weight of property i, and n_i is the exponent for property i, which is set to a value of ± 1. A positive value of n_i was used for standard deviations, as it is desired to minimize the variability, while a negative value of n_i was used for the studied mechanical properties as we would like to maximize mechanical performance. All weights, w_i, were set to 1 for this work, indicating that all properties were considered equally important. The samples produced at 240 °C were excluded from this analysis due to the processing challenges experienced at this temperature. The results of this optimization analysis are shown in Table 9, with results color-coded by processing temperature to match previous figures. We also compared the mechanical properties to talc-filled polypropylene. This is a material that is commonly used for injection molded automotive parts such as bumpers, instrument panels, door panels, and mirror housings [36,37]. We chose this as a point of comparison to determine if our recycled material has appropriate properties for automotive applications.

Overall, our analysis shows that 210 °C is the best temperature for injection molding of paper composite material, producing samples with the highest mechanical properties and lowest standard deviations. Higher screw speeds also appear to produce better samples overall, although this is not consistent across the study. The comparison to talc-filled polypropylene also shows that even the "worst" of the injection molded paper composite samples are on par or better than a widely used automotive material. This suggests that even at sub-optimal processing conditions, the paper-polypropylene composite could be used in a wide variety of automotive applications.

 doi:10.20944/preprints202410.1946.v1

Table 9. Results of objective function analysis for injection molded specimens with color-coding to match previous figures (i.e. Figure 5). Comparison data for talc-filled polypropylene was obtained from work by Kant *et al.* [44].

Set Name	Young's Modulus	Ultimate Tensile Strength	Flexural Modulus	Flexural Strength	$f_{obj}(s_j)$
T210-I3	1680 ± 30	46.2 ± 0.3	2770 ± 50	67.4 ± 0.4	5.408
T210-I4	1640 ± 70	45.3 ± 0.9	2740 ± 40	68.2 ± 1.1	6.049
T210-I2	1680 ± 40	45.8 ± 0.4	3000 ± 220	66.8 ± 0.4	6.284
T230-I4	1510 ± 180	42.3 ± 2.3	2900 ± 200	70.6 ± 2.1	6.381
T220-I1	1550 ± 100	44.6 ± 0.6	2800 ± 300	66.6 ± 0.8	6.543
T200-I3	1440 ± 30	45.3 ± 0.5	2770 ± 120	66.0 ± 0.5	6.688
T230-I1	1670 ± 110	43.6 ± 1.1	2800 ± 160	68.3 ± 1.3	7.201
T230-I3	1590 ± 150	42.5 ± 1.4	3040 ± 130	71.0 ± 2.2	7.297
T220-I3	1650 ± 30	44.6 ± 0.4	3000 ± 50	69.8 ± 1.1	7.345
T200-I1	1630 ± 120	46.0 ± 0.8	2900 ± 120	69.9 ± 2.7	8.196
T210-I1	1670 ± 40	46.0 ± 0.4	2810 ± 200	69.1 ± 2.3	8.777
T230-I2	1680 ± 80	44.1 ± 0.6	2760 ± 40	68.4 ± 0.5	9.155
T200-I2	1580 ± 100	45.4 ± 1.0	2670 ± 70	66.6 ± 0.4	9.291
T220-I4	1640 ± 60	44.6 ± 0.4	3090 ± 40	70.4 ± 1.1	9.823
T220-I2	1540 ± 30	44.1 ± 0.4	2610 ± 60	66.7 ± 0.7	10.794
T200-I4	1440 ± 150	45.2 ± 1.3	2690 ± 70	66.4 ± 0.4	12.869
Unfilled PP	447	26.6	2046	22.9	N/A
10% Talc Filled PP	489	25.3	1754	23.8	N/A
20% Talc Filled PP	599	25.3	2484	26.5	N/A
50% Talc Filled PP	946	23.5	7891	33.0	N/A

4. Conclusions

This research investigated the feasibility of mechanically recycling paper fiber-reinforced polypropylene composites using industrially relevant methods. Paper composite laminates were size-reduced and compounded with virgin polypropylene to produce an injection molding compound. This material was then injection molded under various processing conditions to explore the optimal processing parameter windows. The impact of these processing parameters on the thermal, mechanical, and water uptake properties of the resulting composites was studied. Our findings indicate that processing temperature has the most significant impact on the material properties. Higher processing temperatures increased crystallinity, potentially due to a decrease in polypropylene molecular weight through chain scission. Additionally, higher processing temperatures resulted in increased degradation of the paper fibers, negatively impacting the mechanical performance of the composite. The injection rate had a less significant impact on the material properties than processing temperature; however, increasing the injection rate did appear to damage the paper fibers via shear effects. Neither the composites' water uptake nor thermal stability changed as a function of processing conditions. The mechanical strength of the composite decreased with increasing processing temperature. However, the mechanism was different for tensile and flexural behavior. Tensile strength decreased linearly, while flexural strength remained constant until a temperature threshold was exceeded. Neither tensile nor flexural stiffness changed significantly as a function of processing conditions. Ultimately, the results of this research demonstrate a high potential for mechanical recycling of the paper fiber-reinforced polypropylene

composites into an automotive grade injection molding compound and that the material system has a wide injection molding processing window.

Supplementary Materials: The following supporting information can be downloaded at the website of this paper posted on Preprints.org. Table S1: Thermal analysis data summary, Table S2: Mechanical properties and water uptake data summary, Table S3: P-values for multivariate correlation analysis Figure S1: TGA plot for samples molded at an injection rate of 2 in^3/s but different temperatures., Figure S2: TGA Results (a) T_{50} and (b) Residual mass for samples molded at different injection rate and temperatures, Figure S3: DSC analysis JMP plots, Figure S4: TGA Analysis JMP Plots, Figure S5: Mechanical Properties JMP Plots.

Author Contributions: Conceptualization: C.G., D.H., H.M., J.M., M.K.; Methodology: C.G., D.H., D.K., J.M., M.M.; Formal Analysis: C.G., M.M.; Investigation: C.G., D.H., J.G., J.M., M.M.; Resources: D.H., J.M.; Data Curation: C.G., M.M.; Writing – Original Draft Preparation: C.G., M.M.; Writing – Review & Editing: D.H., D.K., H.M., J.G., M.M.; Visualization: C.G., M.M.; Supervision: D.H., D.K.; Project Administration: D.H.; Funding Acquisition: D.H., H.M., M.K.

Funding: Research reported in this publication was supported, in part, by Volkswagen Group of America, Inc. (VWGoA) and by The University of Tennessee's Faculty Student Research Award.

Data Availability Statement: Data is contained within the article and supplementary material.

Acknowledgments: Research reported in this publication was supported, at least in part, by Volkswagen Group of America, Inc. (VWGoA). The content of this research is solely the authors' responsibility and does not necessarily represent the official views of VWGoA. The authors would also like to thank Domtar Corporation, part of the Paper Excellence Group of companies, for donating the market pulp used in this work.

Conflicts of Interest: The authors declare the following financial interests/personal relationships which may be considered as potential competing interests: David P. Harper reports financial support was provided by Volkswagen Group of America Inc. David P. Harper reports a relationship with Volkswagen Group of America Inc that includes funding grants. Cecile Grubb reports a relationship with Volkswagen Group of America Inc that includes employment. Mahshid Mokhtarnejad reports a relationship with Volkswagen Group of America that includes employment. Marton Kardos reports a relationship with Volkswagen Group of America Inc that includes employment. Hendrik Mainka reports a relationship with Volkswagen Group of America Inc that includes employment. David P. Harper has patent pending to University of Tennessee Research Foundation. Marton Kardos has patent pending to Volkswagen Group of America. Hendrik Mainka has patent pending to Volkswagen Group of America. If there are other authors, they declare that they have no known competing financial interests or personal relationships that could have appeared to influence the work reported in this paper.

References

1. Koronis, G.; Silva, A.; Fontul, M. Green Composites: A Review of Adequate Materials for Automotive Applications. *Compos. Part B Eng.* **2013**, *44*, 120–127, doi:10.1016/j.compositesb.2012.07.004.
2. Khalid, M.Y.; Al Rashid, A.; Arif, Z.U.; Ahmed, W.; Arshad, H.; Zaidi, A.A. Natural Fiber Reinforced Composites: Sustainable Materials for Emerging Applications. *Results Eng.* **2021**, *11*, 100263, doi:10.1016/j.rineng.2021.100263.
3. Khan, T.; Hameed Sultan, M.T.B.; Ariffin, A.H. The Challenges of Natural Fiber in Manufacturing, Material Selection, and Technology Application: A Review. *J. Reinf. Plast. Compos.* **2018**, *37*, 770–779, doi:10.1177/0731684418756762.
4. Nassar, M.M.A.; Alzebdeh, K.I.; Pervez, T.; Al-Hinai, N.; Munam, A. Progress and Challenges in Sustainability, Compatibility, and Production of ECO-COMPOSITES : A STATE-OF-ART Review. *J. Appl. Polym. Sci.* **2021**, *138*, 51284, doi:10.1002/app.51284.
5. Haag, K.; Padovani, J.; Fita, S.; Trouvé, J.-P.; Pineau, C.; Hawkins, S.; De Jong, H.; Deyholos, M.K.; Chabbert, B.; Müssig, J.; et al. Influence of Flax Fibre Variety and Year-to-Year Variability on Composite Properties. *Ind. Crops Prod.* **2017**, *98*, 1–9, doi:10.1016/j.indcrop.2016.12.028.
6. Naidu, A.L.; Rao, P.R. A Review on Chemical Behavior of Natural Fiber Composites. *Int. J. Chem. Sci.* **2016**, *14*, 2223–2238.

7. Injection Molding of Natural Fiber Reinforced Composites. In *Green Biorenewable Biocomposites*; Thakur, V.K., Kessler, M.R., Eds.; Apple Academic Press, 2016; pp. 293–308 ISBN 978-0-429-17420-9.
8. Jahnz, A.; Dejond, C. Circular Economy: Improving Design and End-of-Life Management of Cars for More Resource-Efficient Automotive Sector 2023.
9. Grubb, C.A.; Kardos, M.; Webb, C.; Mainka, H.; Keffer, D.J.; Harper, D.P. Manufacturing and Characterization of Polypropylene-Paper Composites for Automotive Applications. In Proceedings of the SAMPE 2023; NA SAMPE, 2023.
10. Dunne, R.; Desai, D.; Sadiku, R.; Jayaramudu, J. A Review of Natural Fibres, Their Sustainability and Automotive Applications. *J. Reinf. Plast. Compos.* **2016**, *35*, 1041–1050, doi:10.1177/0731684416633898.
11. K., B.; Cetecioglu, Z.; Ince, O. Pollution Prevention in the Pulp and Paper Industries. In *Environmental Management in Practice*; Broniewicz, E., Ed.; InTech, 2011 ISBN 978-953-307-358-3.
12. Sithole, B.B. Pulp and Paper. *Anal. Chem.* **1995**, *67*, 87R-95R.
13. Zhao, X.; Copenhaver, K.; Wang, L.; Korey, M.; Gardner, D.J.; Li, K.; Lamm, M.E.; Kishore, V.; Bhagia, S.; Tajvidi, M.; et al. Recycling of Natural Fiber Composites: Challenges and Opportunities. *Resour. Conserv. Recycl.* **2022**, *177*, 105962, doi:10.1016/j.resconrec.2021.105962.
14. Augier, L.; Sperone, G.; Vaca-Garcia, C.; Borredon, M.-E. Influence of the Wood Fibre Filler on the Internal Recycling of Poly(Vinyl Chloride)-Based Composites. *Polym. Degrad. Stab.* **2007**, *92*, 1169–1176, doi:10.1016/j.polymdegradstab.2007.04.010.
15. Beg, M.D.H.; Pickering, K.L. Reprocessing of Wood Fibre Reinforced Polypropylene Composites. Part I: Effects on Physical and Mechanical Properties. *Compos. Part Appl. Sci. Manuf.* **2008**, *39*, 1091–1100, doi:10.1016/j.compositesa.2008.04.013.
16. Nadali, E.; Layeghi, M.; Ebrahimi, G.; Naghdi, R.; Jonoobi, M.; Khorasani, M.M.; Mirbagheri, Y. Effects of Multiple Extrusions on Structure-Property Performance of Natural Fiber High-Density Polyethylene Biocomposites. *Mater. Res.* **2018**, *21*, doi:10.1590/1980-5373-mr-2017-0301.
17. Soccalingame, L.; Perrin, D.; Bénézet, J.-C.; Bergeret, A. Reprocessing of UV-Weathered Wood Flour Reinforced Polypropylene Composites: Study of a Natural Outdoor Exposure. *Polym. Degrad. Stab.* **2016**, *133*, 389–398, doi:10.1016/j.polymdegradstab.2016.09.011.
18. Correa-Aguirre, J.P.; Luna-Vera, F.; Caicedo, C.; Vera-Mondragón, B.; Hidalgo-Salazar, M.A. The Effects of Reprocessing and Fiber Treatments on the Properties of Polypropylene-Sugarcane Bagasse Biocomposites. *Polymers* **2020**, *12*, 1440, doi:10.3390/polym12071440.
19. Fazita, M.R.; Jayaraman, K.; Bhattacharyya, D.; Hossain, Md.; Haafiz, M.K.; H.P.S., A. Disposal Options of Bamboo Fabric-Reinforced Poly(Lactic) Acid Composites for Sustainable Packaging: Biodegradability and Recyclability. *Polymers* **2015**, *7*, 1476–1496, doi:10.3390/polym7081465.
20. Uitterhaegen, E.; Parinet, J.; Labonne, L.; Mérian, T.; Ballas, S.; Véronèse, T.; Merah, O.; Talou, T.; Stevens, C.V.; Chabert, F.; et al. Performance, Durability and Recycling of Thermoplastic Biocomposites Reinforced with Coriander Straw. *Compos. Part Appl. Sci. Manuf.* **2018**, *113*, 254–263, doi:10.1016/j.compositesa.2018.07.038.
21. Graupner, N.; Albrecht, K.; Ziegmann, G.; Enzler, H.; Muessig, J. Influence of Reprocessing on Fibre Length Distribution, Tensile Strength and Impact Strength of Injection Moulded Cellulose Fibre-Reinforced Polylactide (PLA) Composites. *Express Polym. Lett.* **2016**, *10*, 647–663, doi:10.3144/expresspolymlett.2016.59.
22. Wang, S.; Zhang, J. Effect of Nucleating Agent on the Crystallization Behavior, Crystal Form and Solar Reflectance of Polypropylene. *Sol. Energy Mater. Sol. Cells* **2013**, *117*, 577–584, doi:10.1016/j.solmat.2013.07.033.

23. Bourmaud, A.; Åkesson, D.; Beaugrand, J.; Le Duigou, A.; Skrifvars, M.; Baley, C. Recycling of L-Poly-(Lactide)-Poly-(Butylene-Succinate)-Flax Biocomposite. *Polym. Degrad. Stab.* **2016**, *128*, 77–88, doi:10.1016/j.polymdegradstab.2016.03.018.
24. Tajvidi, M.; Takemura, A. Recycled Natural Fiber Polypropylene Composites: Water Absorption/Desorption Kinetics and Dimensional Stability. *J. Polym. Environ.* **2010**, *18*, 500–509, doi:10.1007/s10924-010-0215-y.
25. Grubb, C.A.; Keffer, D.J.; Webb, C.D.; Kardos, M.; Mainka, H.; Harper, D.P. Paper Fiber-Reinforced Polypropylene Composites from Nonwoven Preforms: A Study on Compression Molding Optimization from a Manufacturing Perspective. *Compos. Part Appl. Sci. Manuf.* **2024**, *185*, 108339, doi:10.1016/j.compositesa.2024.108339.
26. Litster, J.; Ennis, B. *The Science and Engineering of Granulation Processes*; Particle Technology Series; Springer Netherlands: Dordrecht, 2004; Vol. 15; ISBN 978-90-481-6533-9.
27. Agassant, J.-F.; Arda, D.R.; Combeaud, C.; Merten, A.; Münstedt, H.; Mackley, M.R.; Robert, L.; Vergnes, B. Polymer Processing Extrusion Instabilities and Methods for Their Elimination or Minimisation. *Int. Polym. Process.* **2006**, *21*, 239–255, doi:10.3139/217.0084.
28. Zhang, M.; Guo, B.-H.; Xu, J. A Review on Polymer Crystallization Theories. *Crystals* **2016**, *7*, 4, doi:10.3390/cryst7010004.
29. González-González, V.A.; Neira-Velázquez, G.; Angulo-Sánchez, J.L. Polypropylene Chain Scissions and Molecular Weight Changes in Multiple Extrusion. *Polym. Degrad. Stab.* **1998**, *60*, 33–42, doi:10.1016/S0141-3910(96)00233-9.
30. Zhang, B.; Chen, J.; Ji, F.; Zhang, X.; Zheng, G.; Shen, C. Effects of Melt Structure on Shear-Induced β-Cylindrites of Isotactic Polypropylene. *Polymer* **2012**, *53*, 1791–1800, doi:10.1016/j.polymer.2012.02.023.
31. Bednarek, W.H.; Paukszta, D.; Szostak, M.; Szymańska, J. Fundamental Studies on Shear-Induced Nucleation and Beta-Phase Formation in the Isotactic Polypropylene—Effect of the Temperature. *J. Polym. Res.* **2021**, *28*, 439, doi:10.1007/s10965-021-02652-5.
32. Jung, M.R.; Horgen, F.D.; Orski, S.V.; Rodriguez C., V.; Beers, K.L.; Balazs, G.H.; Jones, T.T.; Work, T.M.; Brignac, K.C.; Royer, S.-J.; et al. Validation of ATR FT-IR to Identify Polymers of Plastic Marine Debris, Including Those Ingested by Marine Organisms. *Mar. Pollut. Bull.* **2018**, *127*, 704–716, doi:10.1016/j.marpolbul.2017.12.061.
33. Qian, S.; Igarashi, T.; Nitta, K. Thermal Degradation Behavior of Polypropylene in the Melt State: Molecular Weight Distribution Changes and Chain Scission Mechanism. *Polym. Bull.* **2011**, *67*, 1661–1670, doi:10.1007/s00289-011-0560-6.
34. Łojewska, J.; Miśkowiec, P.; Łojewski, T.; Proniewicz, L.M. Cellulose Oxidative and Hydrolytic Degradation: In Situ FTIR Approach. *Polym. Degrad. Stab.* **2005**, *88*, 512–520, doi:10.1016/j.polymdegradstab.2004.12.012.
35. Łojewska, J.; Missori, M.; Lubańska, A.; Grimaldi, P.; Zięba, K.; Proniewicz, L.M.; Congiu Castellano, A. Carbonyl Groups Development on Degraded Cellulose. Correlation between Spectroscopic and Chemical Results. *Appl. Phys. A* **2007**, *89*, 883–887, doi:10.1007/s00339-007-4220-5.
36. Chen, Z.; Hu, T.Q.; Jang, H.F.; Grant, E. Multivariate Analysis of Hemicelluloses in Bleached Kraft Pulp Using Infrared Spectroscopy. *Appl. Spectrosc.* **2016**, *70*, 1981–1993, doi:10.1177/0003702816675363.
37. Lionetto, F.; Del Sole, R.; Cannoletta, D.; Vasapollo, G.; Maffezzoli, A. Monitoring Wood Degradation during Weathering by Cellulose Crystallinity. *Materials* **2012**, *5*, 1910–1922, doi:10.3390/ma5101910.

38. Li, J.; Zhu, Z.; Li, T.; Peng, X.; Jiang, S.; Turng, L. Quantification of the Young's Modulus for Polypropylene: Influence of Initial Crystallinity and Service Temperature. *J. Appl. Polym. Sci.* **2020**, *137*, 48581, doi:10.1002/app.48581.
39. Tsui, N.T.; Paraskos, A.J.; Torun, L.; Swager, T.M.; Thomas, E.L. Minimization of Internal Molecular Free Volume: A Mechanism for the Simultaneous Enhancement of Polymer Stiffness, Strength, and Ductility. *Macromolecules* **2006**, *39*, 3350–3358, doi:10.1021/ma060047q.
40. Schultz, J.M. Microstructural Aspects of Failure in Semicrystalline Polymers. *Polym. Eng. Sci.* **1984**, *24*, 770–785, doi:10.1002/pen.760241007.
41. Nugroho, G.; Budiyantoro, C. Optimization of Fiber Factors on Flexural Properties for Carbon Fiber Reinforced Polypropylene. *J. Compos. Sci.* **2022**, *6*, 160, doi:10.3390/jcs6060160.
42. Leguillon, D.; Martin, É.; Lafarie-Frenot, M.-C. Flexural vs. Tensile Strength in Brittle Materials. *Comptes Rendus Mécanique* **2015**, *343*, 275–281, doi:10.1016/j.crme.2015.02.003.
43. Schober, P.; Boer, C.; Schwarte, L.A. Correlation Coefficients: Appropriate Use and Interpretation. *Anesth. Analg.* **2018**, *126*, 1763–1768, doi:10.1213/ANE.0000000000002864.
44. Kant, S.; Urmila; Kumar, J.; Pundir, G. Study of Talc Filled Polypropylene - A Concept for Improving Mechanical Properties of Polypropylene. *Int. J. Res. Eng. Technol.* **2013**, *02*, 411–415, doi:10.15623/ijret.2013.0204001.